Fusion Engineering and Design 170 (2021) 112457

Contents lists available at ScienceDirect

Fusion Engineering and Design

journal homepage: www.elsevier.com/locate/fusengdes

Prototype mitre bends of the ex-vessel waveguide system for the ITER upper launcher: Thermal hydraulic simulations and experiments with off-center mm-wave beams

A. Xydou [a,*], T. Goodman [a], R. Chavan [a], M. Vagnoni [a], H. Torreblanca [a], M. Cavinato [b]

[a] Ecole Polytechnique Fédérale de Lausanne (EPFL), Swiss Plasma Center (SPC), CH-1015 Lausanne, Switzerland
[b] Fusion for Energy, Josep Pla 2, Torres Diagonal Litoral B3, E-08019 Barcelona, Spain

ARTICLE INFO

Keywords:
Upper launcher
Miter bend
Thermal-hydraulic analysis
Off-centered beams

ABSTRACT

On ITER, long pulse gyrotrons are required as a power source for electron cyclotron heating (ECH) and current drive (CD). The microwaves are guided from the gyrotrons, which are placed far from the Tokamak, into the plasma by transmission lines (TLs) and a launching antenna (launcher). Each of the four ECH Upper launchers features eight waveguide (WG) TLs, with at least 95% of the power from the gyrotrons coupled into in the main HE_{11} mode of the TLs. In the ex-vessel portion of the system between the port-plug closure plate and the isolation valve and diamond window, there are miter bends (MBs) that change the direction of the TL by reflecting the millimeter waves (mm-waves) using mirrors; the mirrors must handle 1.31 MW, 170 GHz, 3600 s pulses. Various MBs perform these reflections at an angle of 90 degrees, or nearly 100 degrees. As a result of the ohmic dissipation, an intensive peaked heat flux appears near the center of the MB mirror and thus, a dedicated cooling system is present to ensure the temperature control of the mirror and housing e.g. [1]. The power that is not found in the HE_{11} mode can cause the beam to be not perfectly centered, resulting in an off-centered heat flux on the mirror surface; as is the case for the experiments described here. This study presents new finite element modeling of such beams, created in CFX of ANSYS Workbench [2], compared to the experimental findings for pulses of 170 GHz, 0.5 MW and 240 s. Monitor points are placed in the same positions as TCs that have been fitted in the mirror close to the heated surface and direct comparison of the temperature values is performed. Through transient simulation the time constants are calculated and compared with those of the experiments.

1. Introduction

The TLs consist of low-loss corrugated circular WGs, which guide the mm-waves from the gyrotrons to the Tokamak [3] and with a maximum power of 1.31 MW for up to 3600 s. MBs are used to change the direction of the TL by reflecting the waves from highly reflective mirrors. The MBs are critical TL components since they are responsible for the dominant losses in a TL. The losses are a combination of ohmic and mode conversion losses [4,5]. The mode conversion losses increase with the increasing content of the high order modes (HOM). A HE_{11} pure mode results in a high transmission efficiency because of its very low ohmic losses as the mode propagates along the WG [6]. The requirement of the HE_{11} mode purity on the ITER TL is more than 95% at the input. An efficient cooling system in the MB body is required [7] in order to remove the generated heat and to keep the MB body and mirror at a reasonable temperature, minimising at the same time the deformation of the reflective center which may affect the mode purity in steady state [8,9].

The SPC has designed and manufactured a 50 mm, cooled, prototype MB which was tested at FALCON [10] to ensure the temperature control of the mirror and housing due to the intensive peaked power density in the middle of the MB mirror. Fluid-dynamic simulations are performed in ANSYS Workbench R3 CFX in order to assess the flow distribution and heat transfer expected in the MB and to compare with the experimental findings.

2. MB cooling design

The corrugated WG MB body and the reflective mirror are made of copper chromium zirconium (CuCrZr) alloy which provides high yield

* Corresponding author.
E-mail address: anastasia.xydou@epfl.ch (A. Xydou).

https://doi.org/10.1016/j.fusengdes.2021.112457
Received 30 November 2020; Received in revised form 12 February 2021; Accepted 4 March 2021
Available online 31 March 2021
0920-3796/© 2021 The Authors. Published by Elsevier B.V. This is an open access article under the CC BY license (http://creativecommons.org/licenses/by/4.0/).

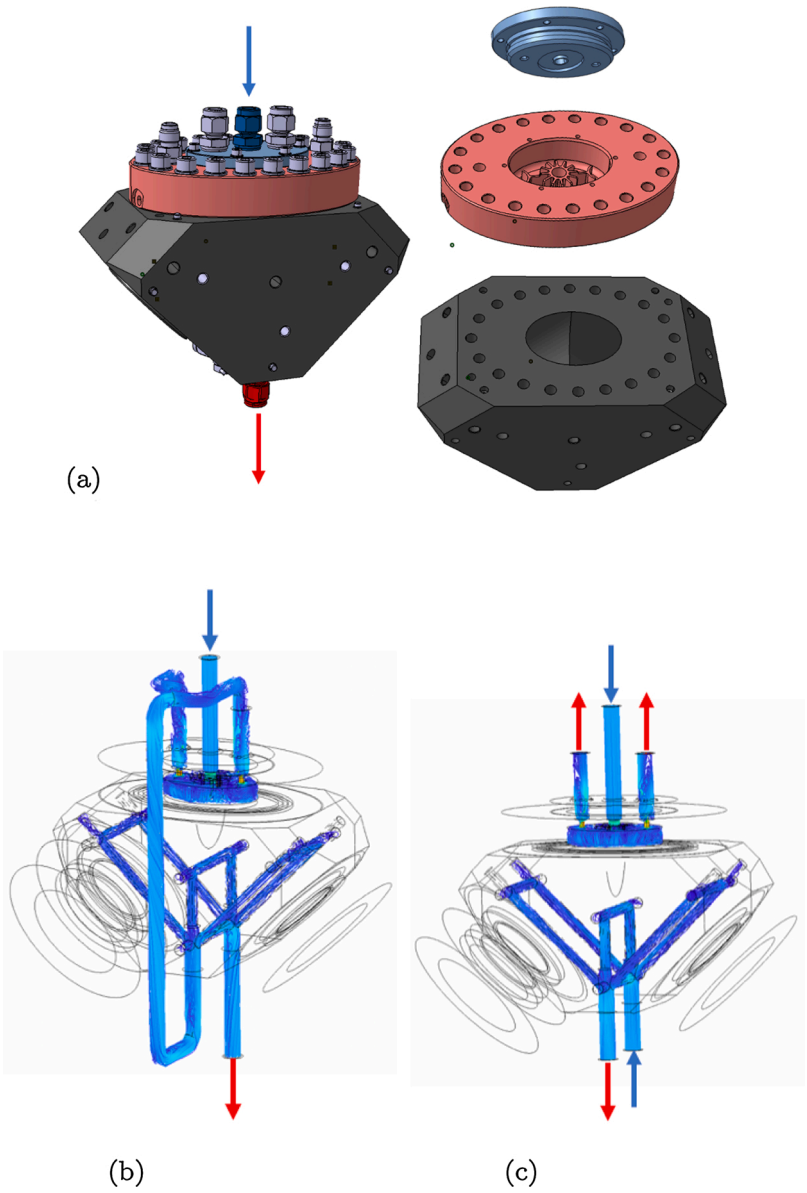

Fig. 1. Corrugate WG MB body and the reflective mirror with the water body.

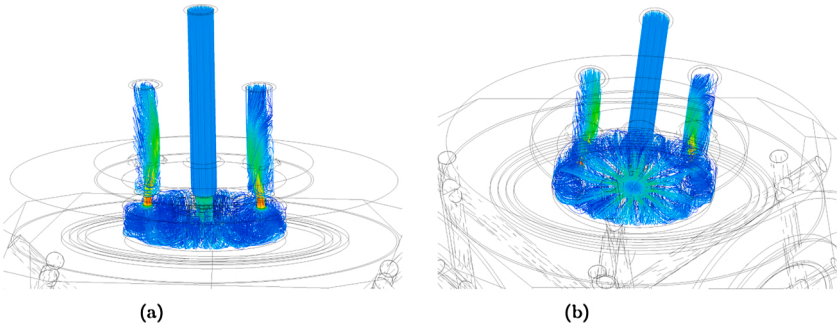

Fig. 2. Detailed view of the water body in the reflective mirror.

strength and only a small reduction in conductivity, relative to pure copper (Cu). Both components are assembled via a bolted connection with a double-metallic seal configuration ensuring Ultra High Vacuum confinement with a maximum leak rate of 10^{-10} Pa m^3 s^{-1} (Fig. 1a). The cooling circuits of the MB mirror and body, following the experimental setup, are connected either in series or in parallel (Fig. 1b and c). In the serial flow, the water is fed on the back side of the mirror through a cap as shown in Fig. 1b; then the flow splits in two as it leaves the mirror and reconnects, externally, in order to reach the MB body. The cooling channels in the body go around the heated surfaces and reconnect,

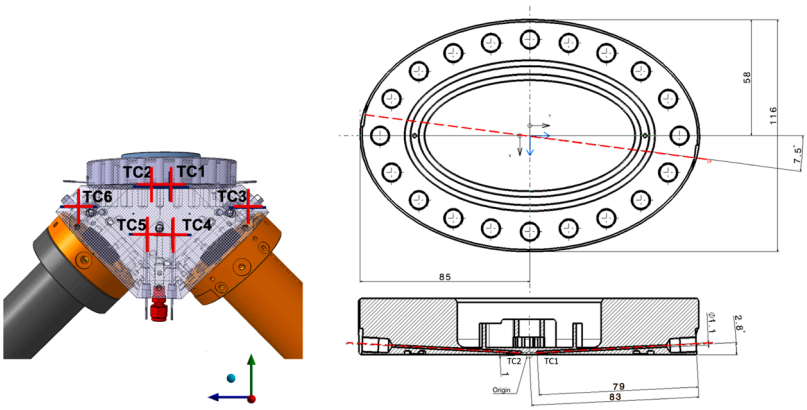

Fig. 3. Detailed view of the TCs in the mirror and the MB body. On the left the TCs are highlighted with crosses while on the right more details are shown for the position of the TC1 and TC2 which are located in the mirror.

internally, to leave the MB body. In the parallel configuration the water is inserted in parallel at the mirror and the body as shown in Fig. 1c. Fig. 2 shows in details the water flow in the mirror.

2.1. Thermocouples (TCs)

The MB is fit with type-K thermocouples (TCs) to allow the comparison of experiments with simulations. Two TCs are inserted in deep-drilled holes 1 mm behind the MB mirror surface and each are 4 mm away from the reflective center of the mirror along a straight line. The TC location line in the Mirror is rotated by 7.5 degrees relative to the horizontal axis (Fig. 3a top), and each hole is tilted by 2.8 degrees relative to the mirror surface as shown in 3 b bottom) – from the reflective center towards the extremities. Additionally, two TCs are inserted near the intersection of the input and output arms of the MB body, and two TCs are inserted near the WG flanges of the MB arms (Fig. 3).

3. Experimental procedure

High power mm-wave heating experiments were carried out using the FALCON test facility with RF pulses of up to 1000 sec. The two TCs embedded in the mirror 4 mm right and left of the reflective center of the mirror, showed an unequal heating which suggested that the RF beam in the experiment is not a purely HE_{11} mode, but rather a combination of HOM and HE_{11}, due to the non-ideal coupling of the gyrotron output beam to the WG (and other possible experimental misalignment).

3.1. Beam pattern phase reconstruction

In order to perform free-space microwave beam profile measurements a wood-lined, aluminum paneled, mm-wave leak tight box was placed at the end of the TL, replacing the load, as shown in Fig. 4a. The reconstructed beam pattern is projected onto the WG modes, which are propagated back to the MB mirror to provide the short pulse input beam intensity. Inside the box, a square target is placed as shown in Fig. 4b and was irradiated from the output microwave beam. The temperature profile (or the corresponding beam-intensity pattern) was recorded using an infrared (IR) camera (Fig. 6), the camera was moved together with the target to maintain perspective. IR images from three different target distances from the WG mouth are used to retrieve the beam phase/amplitude pattern, iteratively. The result is back-propagated to the WG mouth and is projected onto the 16 lowest linearly polarized HOM LP_{mn} modes [11–13] (relative fractions and phases). The fractional mode content is then plotted (the main mode fraction is given in the title as it is much larger than the HOMs). The reconstructed beam profile is shown in Fig. 5a, and the mode distribution is shown in Fig. 5b.

3.2. Burn pattern

As an additional verification to the reconstructed phase, the burn pattern of the RF beam was measured. The MB mirror was replaced by burn paper as shown in Fig. 7a and an absorber was placed against that during the measurement. The RF beam was also radiated from the MB mirror opening onto target absorbers at two distances to make IR images as shown in Fig. 7b. Fig. 8 demonstrates the superposition of the reconstructed beam pattern projected on the mirror surface and the burn pattern.

4. Finite element analysis

ANSYS Workbench 2019 R3 is used for the Finite Element Analysis (FEA), with CFX module for the fluid dynamic (CFD) analysis. The analysed TL, consisted of seven solid and water bodies (Fig. 10). Five of the seven solid bodies are made of CuCrZr: the main body of the MB, its mirror, a short WG of 0.33 m, the load adapter which is water-cooled and allows the short WG to be coupled with RFL.20 [14] and the flange that is used as a gender changer. The long WG of 1.2 m is made of aluminum alloy (Al) and the cap of the Mirror is made of Cu. The temperature variation of the linear properties of Cu and CuCrZr is taken into account based on the ITER material database [15]. The material properties of Al are taken from the default CFX materials database.

4.1. Centered beam

In order to compare with previous analyses [1], initially the distribution of absorbed power on the mirrors is considered as a pure HE_{11} incident wave. The MB mirror receives a circular J_0^2 Bessel function, projected, as a heat flux profile on the mirror, with resistivity as a function of temperature. The heated region is elliptical, since the power is incident at a 45 degrees angle. The peak flux is about 1800 kW/m^2 and varies a little depending on the water flow. Further details about the heat load applied on mirror are given in Appendix A.1. The transmitted power equals 0.465 MW with an enhancement s-factor for power absorption equal to 1.44 (see Appendix A.1). The water flow in this case was in series and a parametric study of the water flow was performed in the range of 0.1 to 0.19 kg/s, for acquiring a better understanding on the cooling performance.

4.2. Off-centered beam

In order to simulate the off-centered beams, the intensity of the

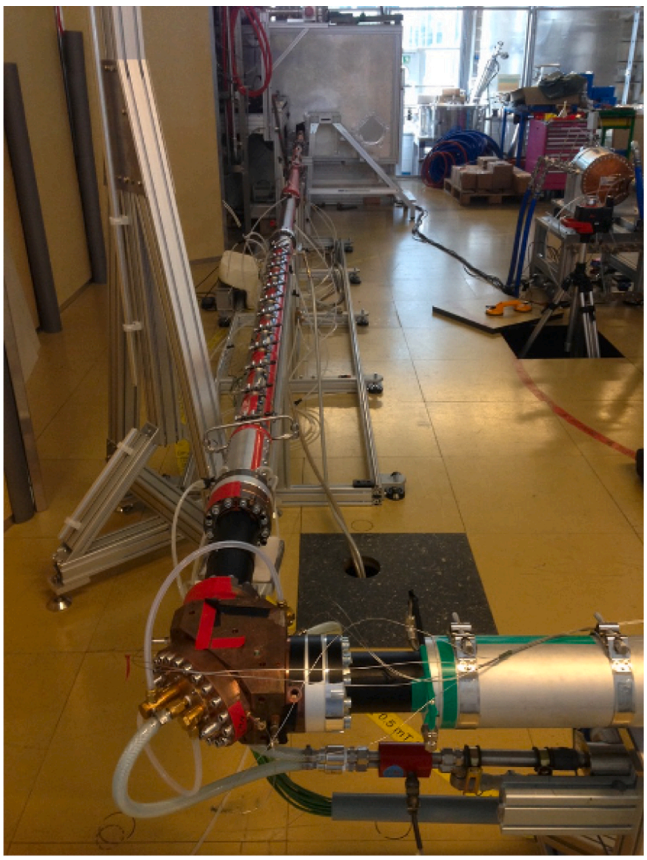

(a)

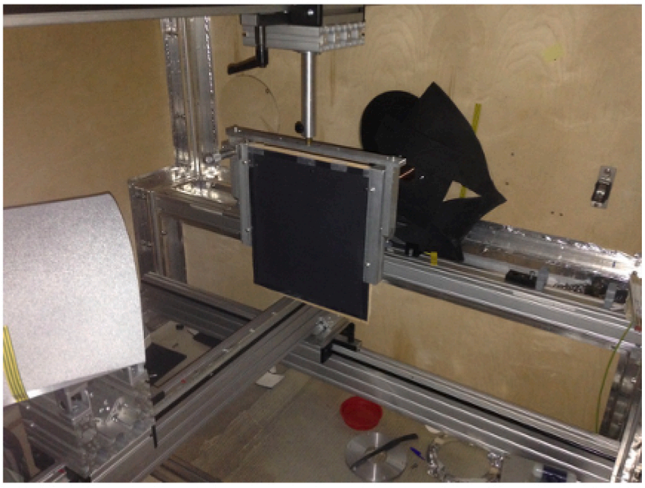

(b)

Fig. 4. Experimental set up for the free-space microwave beam profile measurements.

reconstructed phase which was extracted experimentally (3.1) is imported as a function of *x, y* and *z* coordinates (Fig. 9) and multiplied by the loss factor ($f_{\Omega H}\cdot\cos\frac{\theta}{2}$); finally, it is projected on the mirror surface. For these analyses, both the TL described above and a simpler one without the WGs were used. The simpler one consists of the MB body, mirror and the mirror's cap; its main purpose was to perform several parametric studies with computational efficiency. Both parallel and serial flows were used for these analyses.

In all examined cases, the water flow (parallel/serial) is turbulent and the Shear Stress Transport Model (SST) [16] is chosen as the most accurate to describe the turbulence of the flow at the walls as well as the bulk. The heat loads and boundary conditions of the MB body and the associated WGs are estimates including ~ 0.7% reflections from the RFL.20 and ohmic losses from HE_{11} and scattered power; as in the previous analysis [1,10]. The following section as well as Fig. 10 summarize the boundary conditions of the simulation set up.

4.3. Boundary conditions

- A 8.2 kW/m^2 heat flux is applied on the CuCrZr load adapter contact face and corrugated WG section.
- Convection cooling within the load adapter is applied with the heat transfer coefficient (HTC) equal to 17.2 kW/m^2 for a diameter of 7 mm cooling channel at 20 °C.
- A 5.7 kW/m^2 heat flux is applied on the corrugated CuCrZr WG section.
- A 6.0 kW/m^2 heat flux is applied on the corrugated arms of the MB.
- A 5.9 kW/m^2 heat flux is applied on the CuCrZr gender changer with two female sides (GCff).

The taper is treated in a more approximate way, as it is not part of the device under test, and the details of the cooling are not calculated. Instead, are used:

- A fixed average inner diameter $1/2\cdot(50+63.5)$ mm with a constant 25 °C temperature on the cooled portion of the taper;
- 3.8 kW/m^2 heat flux on the un-cooled corrugated WG sections near the MB and at the far end. The power loading in the taper is an average value for the entire length.

In the simpler configuration with only the Mirror and the MB body, the heat flux applied on the inner faces of the MB body was equal to 13.8 kW/m^2; this derived from a parametric study as well, as will be described later.

4.4. Mesh

The mesh is done with tetrahedrals as shown in Fig. 11. The total number of elements is $2.2\cdot10^7$ and the total number of nodes is $7\cdot10^6$. The inflation layers applied in the external faces of the water body; are used to bridge the inner region between the wall and the fully-developed turbulence region. The first cell size equals to 10^{-5} m, while 15 layers are added with a growth rate equal to 1.15. This approach aims to minimize the Y+ factor, whose maximum value after the iterations equals 11.94.

4.5. Monitor points

In order to capture the temperature values at the same locations as the TCs (2.1), monitor points were added in the pre-processor of the CFX in the MB body. The same pertains to the mirror: points were added in the pre-processor along the line connecting the TC1 and TC2 with 1 mm spacing, as shown in Fig. 12.

5. Results and discussion

The results of temperature on the mirror surface when considering a pure HE_{11} are shown in Fig. 13. The flow rate is 0.18 kg/s in this demonstration. The temperature on a cut view of the mirror is also shown in Fig. 14.

The monitor points placed at the same location as the TCs on the mirror, as well as those in the MB body, show a small asymmetry (±0.3 °C) relative to the reflective center, this is attributed to the small asymmetry on the output cooling (an additional elbow on the right

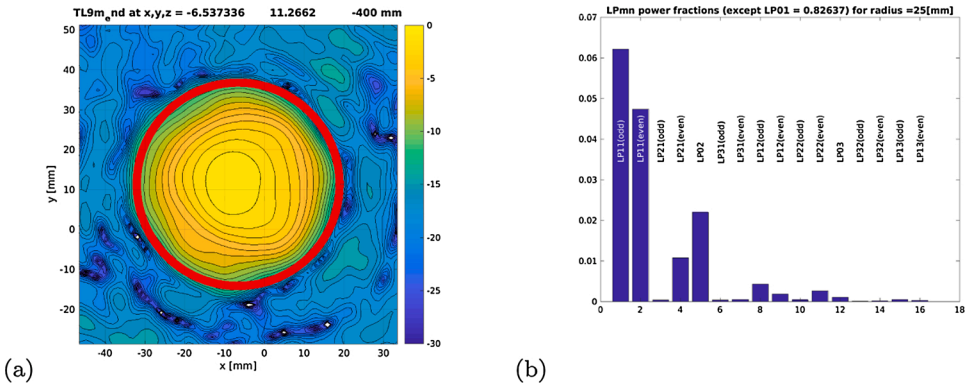

Fig. 5. Beam pattern phase reconstruction.

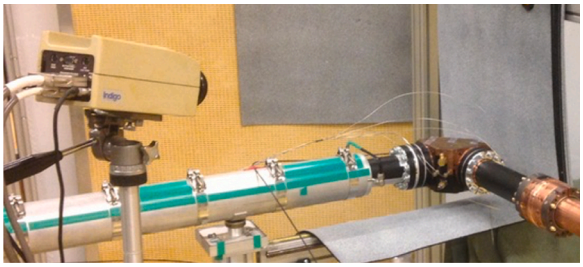

Fig. 6. Setup of IR camera and absorber for the beam spot images.

compared to the left), as well as to the turbulence of the flow. Due to these factors, the peak temperature does not coincide with the geometric center of the mirror, but is moved by 0.5 mm to the positive z direction. This asymmetry is more pronounced in Fig. 14 where the portion of the mirror bolted to the body of the MB is also seen to be warmer due to the higher heat load on the output WG than on the input WG.

Fig. 15 compares the temperature points extracted from the mirror surface to the points extracted from 1mm bellow the surface (same location as the TCs) for variable flow rate values. The temperature values extracted from the mirror surface in all examined cases, show only slightly higher values ($+5\,^{\circ}C$) than the values extracted from the points placed 1 mm below (Fig. 3). The cooling design is effective for preventing the overheating of the MB components.

Fig. 16 presents the temperature profile on the mirror when using the reconstructed beam pattern and the same cooling and WG/Body loading parameters as for the centered case (transmitted power Pt = 465 kW, s-factor = 1.44 and serial flow rate = 0.18 kg/s). Fig. 17 compares the results of the centered beam with the off-centered beam.

The difference in temperature between the two mirror TCs is partly reproduced by the simulations; however, there is still some difference between the ΔT deriving from the experiment and the one from the simulation. This may be explained by the s-factor used in the simulations and the variance of the experimental data from shot to shot. To pin down the s-factor, several further parametric studies were performed and compared to a large experimental data set in which the flow rate was 0.15 kg/s and the flow was in series.

Additionally, the flow in the experimental set up was put in parallel to allow separate calorimetry of the mirror and body circuits. Similarly, in simulations, parallel flow allows different combinations of flow rates to be applied in order to identify the heat flow direction between the MB body and the mirror. For computational efficiency, the simpler model (without adjacent WGs) was used.

A parametric scan was made of the heat flux in the arms of the MB body (5 to 40 kW/m^2) to find the value needed to replicate the heat flow found in the full model from the body into the mirror across the bolted connection surface: this value is 13.8 kW/m^2. From this scan it is found that the temperatures at the mirror TCs do not depend on the heat flux in the body, nor the body temperature; they are independent of the flow rate in the body.

For this reason, the transmitted power scan was performed in the simulations using the body flow rate of 0.082 kg/s, measured for the parallel flow configuration, but with 0.15 kg/s in the mirror (instead of the measured parallel flow rate of 0.18 kg/s) to match the data-set value.

The examined power range was 200–1000 kW with the s-factor = 1. Fig. 18 presents the temperature results on the monitor points placed

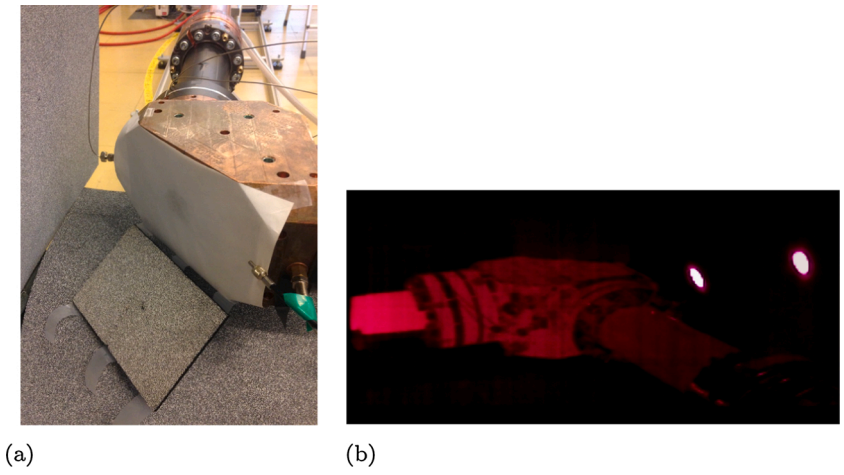

Fig. 7. Detailed pictures from the extraction of the burn pattern.

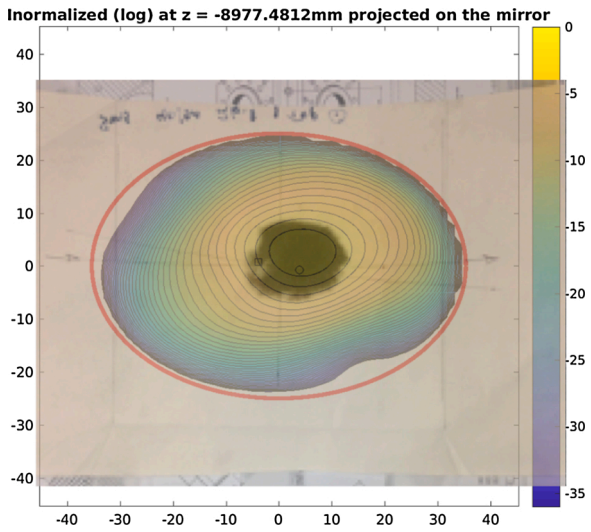

Fig. 8. Projected beam intensity on the mirror surface (log) overlaid with the experimental burn pattern.

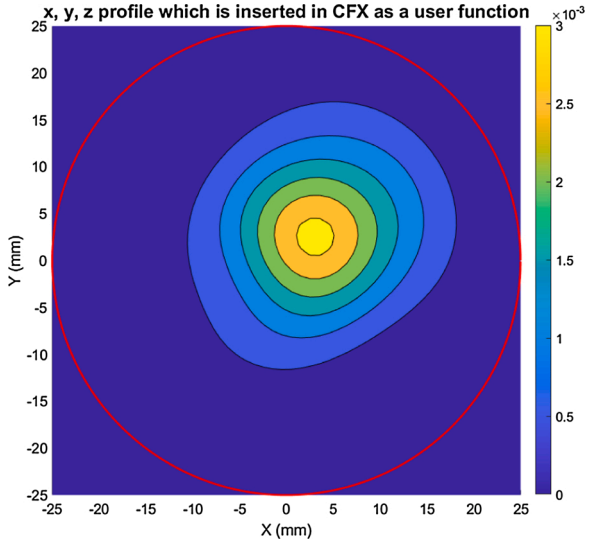

Fig. 9. Beam intensity in the WG (linear) as inserted in CFX.

1mm below the mirror surface. Taking the ΔT (= $T_{steady\ state}$ − T_0) of the monitor points 4 mm right and left of the reflective center (same location with the tips of the TCs) the linear regressions shown in Fig. 19 are derived. The fits to the simulations are shown with the thick green lines and are compared with the experimental data fits. The ratio of the slopes of the simulation and experimental fits provide the s-factor of 1.06. Note that the independent variable, power, is plotted on the *y*-axis to emphasize the possibility to use the MB mirror with embedded TCs as a power monitor, without necessarily resorting to MB calorimetry, once a cross-calibration with the calorimetric load is performed. Alternately, if the s-factor and the beam profile at the mirror are known, *a priori*, simulations can provide the calibration.

Though the data in Fig. 18 are for pulses 20 s or longer, the good

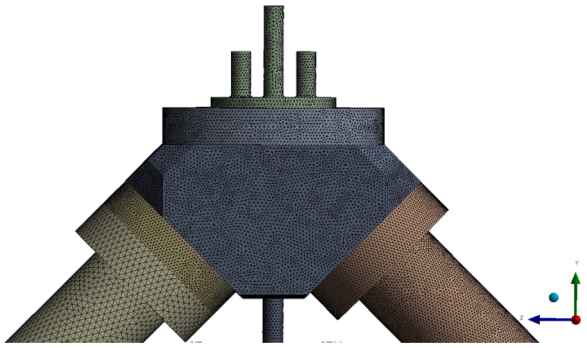

Fig. 11. Mesh overview of the TL.

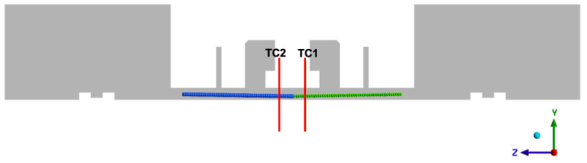

Fig. 12. Monitor points on the mirror along the line connecting the TC1 and TC2 with 1 mm spacing.

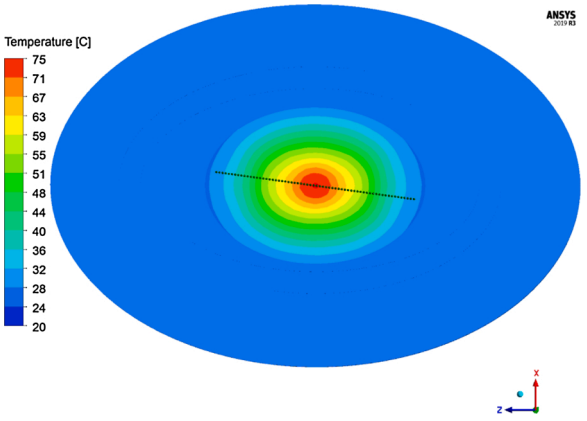

Fig. 13. Temperature results on the mirror surface from the flow rate case equal to 0.18 kg/s. The points shown here, used in each examined case of the flow rate to extract the temperature.

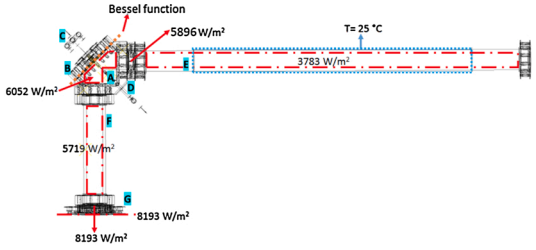

(a)

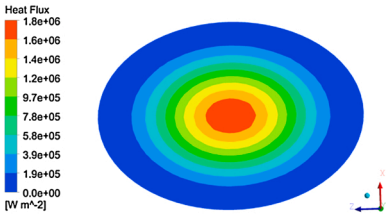

(b)

Fig. 10. Schematic illustration of the TL and heat loads applied on the several components on the left and on the right an example of the heat flux applied on the mirror for the centered beam case.

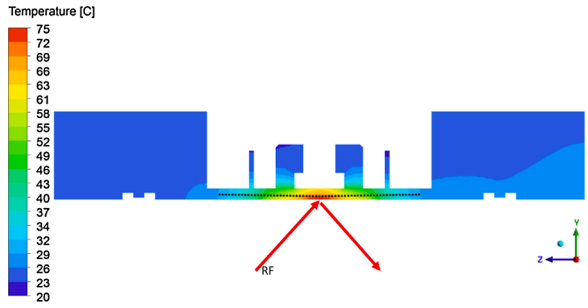

Fig. 14. Temperature results shown on the cut view of the mirror. The points shown here, used in each examined case of the flow rate to extract the temperature. The red arrow shows the RF direction. (For interpretation of the references to color in this figure legend, the reader is referred to the web version of this article.)

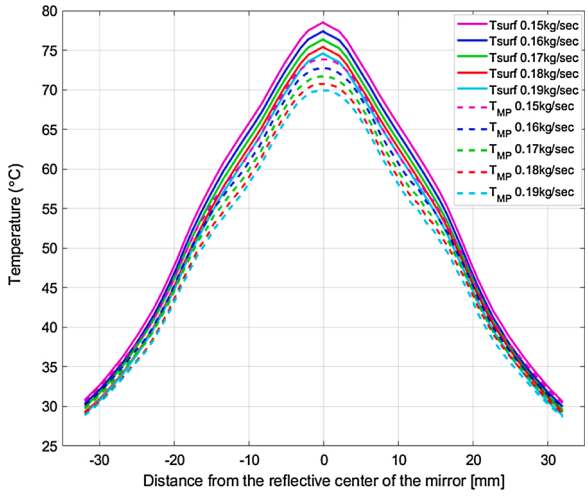

Fig. 15. Temperature values extracted from the points as shown in Figs. 13 and 14 for different cases of flow rates, for serial flow and pure HE_{11} mode.

cooling efficiency and nearness of the TCs to the mirror surface provide a rapid response time that can be used at shorter pulse length to give the power. Fig. 20 compares ΔT for TC2 to the RF signal received from a commercial power monitor miter bend (PMMB).[1] The flow rate in the mirror for this shot is increased to 0.18 kg/s, so the temperature-to-power conversion is not the same as is in Fig. 18, but is based on a separate cross-calibration effort; nevertheless, the conversion slope in Fig. 18 linearly-scaled by the ratio of the flow rates (0.18/0.15) would have provided a reasonably good estimate (within ∼ 5%) even without re-calibration.

Transient analysis of the full configuration with the off centered beam was performed. The parameters of Pt = 440 kW, s-factor = 1.06, mass flow rates $\dot{m}_{\text{mirror}} = 0.18$ kg/s and $\dot{m}_{\text{body}} = 0.082$ kg/s (as in the experiments) were used, while the heat load in the other components were as listed in 4.3. The total time duration equals 100 sec with a time-step of 1 s. In the experiment, the MB mirror stabilises with a time constant of <1 s. Fig. 21 shows a comparison between the results of a similar, shorter, higher time-resolution, transient simulation for the monitor points placed in the mirror in the same location as the TCs.

Fig. 22 presents on the left, the experimental measurement of the temperature in the MB body, and on the right, the simulation results of

[1] a phased array of small, highly-attenuating, vacuum-sealed, coupling holes in a MB mirror with an appropriately mounted receiving antenna and Schottky diode.

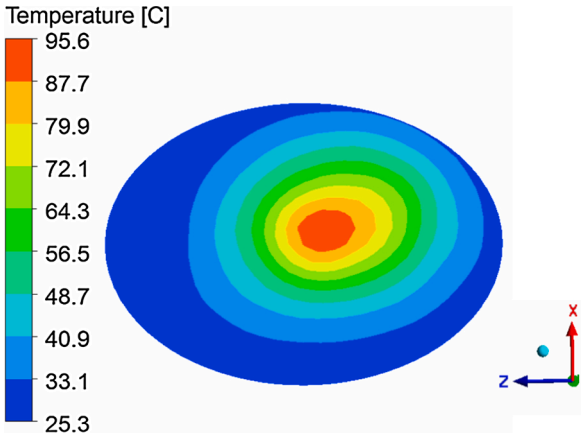

Fig. 16. Temperature profile on the mirror surface for the off centered beam with serial flow and flow rate equal to 0.18 kg/s.

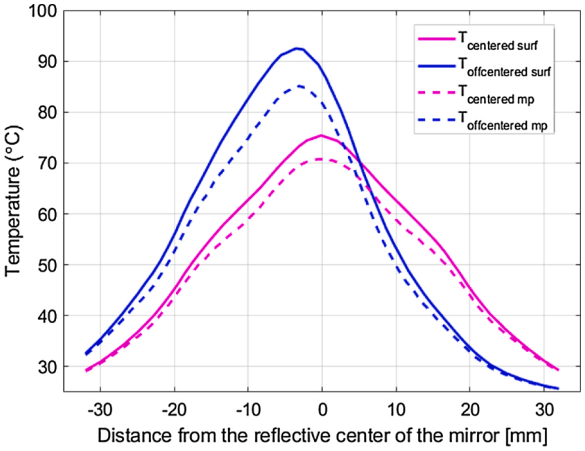

Fig. 17. Temperature values extracted from the mirror surface and from monitor points below the surface for the off centered beams with flow rate equal to 0.18 kg/s, compared to the centered case. The maximum temperature is located on the negative *z*-axis and is in accordance with Fig. 16.

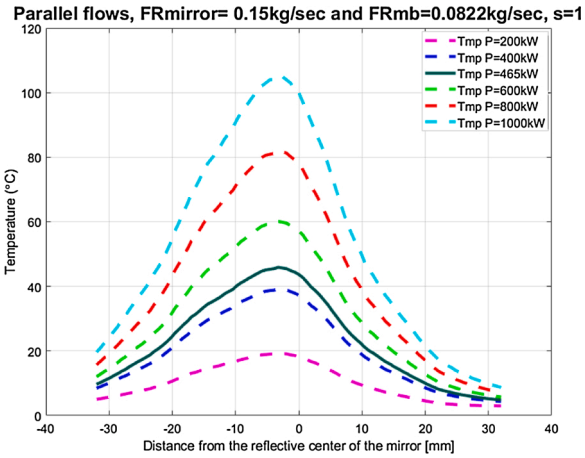

Fig. 18. Temperature extracted from the TCs of the mirror for different values of the transmitted power. The water flows in parallel at mirror and MB body with rates equal to 0.15 kg/s and 0.0822 kg/s, respectively.

the temperature from the monitor points placed in the MB body at same location as the TCs. The parameters derived from the exponential fitting $\Delta T = \alpha(1 - \exp(-t/\tau))$, where τ is the time constant (sec), are listed in Table 1 for both the simulation and experiment.

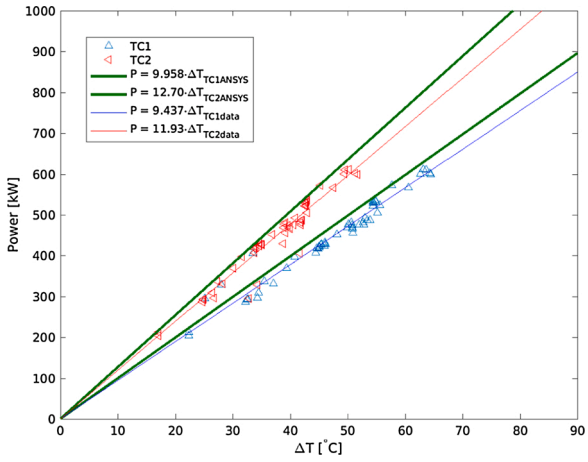

Fig. 19. Based on the results in Fig. 18, the ΔT of the TCs tips 4 mm right and left of the reflective center with $T_0 = 20\,^{\circ}C$ are plotted versus the transmitted power (green curves). These are compared to the FALCON experimental data (points) and associated linear fits. (For interpretation of the references to color in this figure legend, the reader is referred to the web version of this article.)

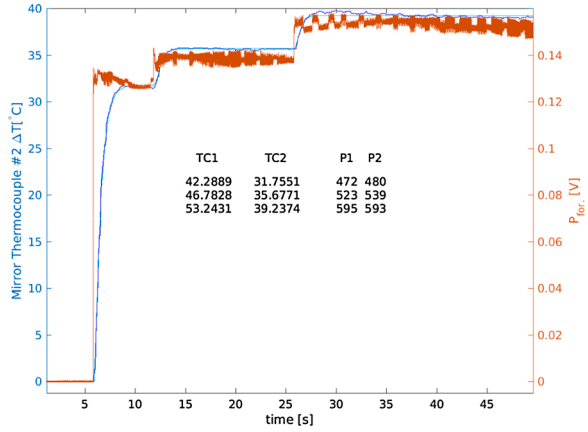

Fig. 20. Comparison of embedded-TC mirror and PMMB mirror response time to steps in the transmitted power. The insert shows the fit temperatures for both TCs and the associated derived powers. TC2 data in (blue) and TC fit (cyan) are nearly superposed. The time constant at each step is 0.5 ± 0.1 s; whereas, the RF forward power diode ($P_{for.}$) from the PMMB (red) shows ms response time. (For interpretation of the references to color in this figure legend, the reader is referred to the web version of this article.)

The time constants derived from the simulation are comparable with the experiments only for the inner corner of the MB legs (TC4 and TC5). All TCs embedded in the MB body are affected by the heat load applied both in MB legs and the adjacent WGs. The discrepancy found in the time constants between simulations and experiments, especially for the TC3 and TC6 show that further analysis is needed to quantify the heat flux coming from the adjacent WGs to the MB body, in particular, because none of these is independently known. The longer time constants found in the simulations benefit from the fact that simulation times are longer than the experimental pulse length (the simulation includes a simple power step): the time constants are significantly longer than the experimental pulse length in this case. Experimentally, longer pulses most often result in non-step-like gyrotron power input to the MB, and are further complicated by a re-circulation of the cooling water in the MB circuits. Moreover, whereas the heat-flux to the mirror is relatively well-known, the heat fluxes in the MB legs and WGs is not yet well quantified. Nevertheless, the good fit to the corner TCs encourages the further investigation.

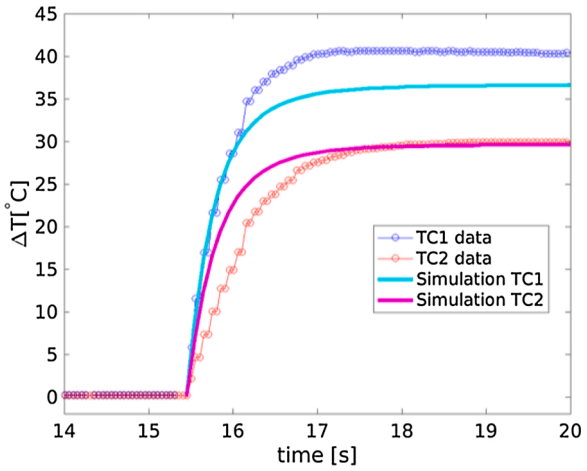

Fig. 21. Comparison of the transient response of the TCs, TC1 and TC2 in the mirror, and the transient response at the monitor points 4 mm right and left of the reflective center (i.e. the TC locations).

6. Conclusions

Thermal hydraulic analyses were performed for the cooling design of the MB mirror and body with the CFX of Ansys Workbench. The heat generated from the microwaves is applied as a heat flux on the mirror surface. A perfectly-centered beam is used to benchmark the present model with previous calculations. Unexpectedly, measurements from two TCs embedded in the mirror just behind the reflecting surface and 4 mm to either side of the mirror's geometric center show significantly different temperatures. Therefore, the cooling performance with an off-centered input beam is analysed.

The input heat flux is derived from experimental free-space intensity measurements taken 9 m downstream from the MB. These are used for phase-retrieval followed by projection of the resulting complex electric field pattern on the modes of the WG and subsequent back-propagation of that mode mixture to the MB mirror location. Steady state analysis is used for most of the calculations and the parametric studies; since the mirror, which is the most important component, reaches steady state rather quickly. Transient analysis is also performed for the case of the off-centered heat flux in order to compare with the experimental measurements.

The heat transfer coefficient (HTC) values are extracted from the simulation by using the steady-state temperature rise of the water at each outlet. The HTC in the cooling channels of the MB body with $\dot{m} = 0.082$ kg/s is found equal to an average value of 3.5 kW/(m^{2}K), and in the cooling cavity of the mirror with $\dot{m} = 0.18$ kg/s, the HTC is found equal to an average value of 11.6 kW/(m^{2}K).

It is to be expected that in TLs in which higher order modes exist, either due to a misaligned input beam, or cummulative misalignments and manufacturing limitations, the beams reflected from the MB mirrors will be off-centered, resulting in off-centered heat generation on the mirror surface. Therefore, it is very important to eliminate asymmetries from the design itself, the cooling circuits shall be 100% symmetric. TCs embedded in the mirror can be used as a power monitor once calibrated by simulation, or after cross-calibration to a calorimetric load. The time response is expected to be fast enough to be able to detect a mode-jump or other loss of power in the gyrotron, allowing shutdown of the high voltage to prevent damage to the gyrotron. This simple diagnostic does not require vacuum windows to allow power to reach an RF diode, as is required for other types of PMMBs.

The TCs are also a very useful diagnostic for the beam localization on the mirror surface. The number of TCs should ideally be greater than two; e.g. placing four TCs in quadrants around the mirror as close to the mirror surface as possible, would allow detection and localization of an

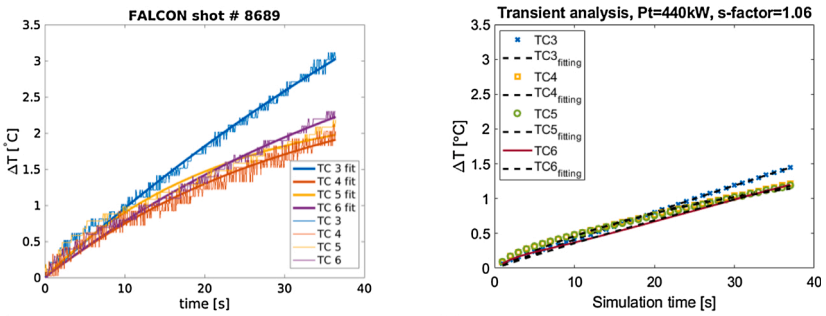

Fig. 22. Comparison of the temperature rise of the TCs on the MB body between experimental measurements and simulations.

Table 1
Fitting parameters for the temperature variation of the monitor points in the simulation and of the TCs in the experiment, placed on the MB body (Fig. 3).

Monitor points	α_{simul}	τ_{simul} (s)	α_{exp}	τ_{exp} (s)
TC3	11.19	267.5	8.8624	87.106
TC4	1.658	30.4	2.8542	32.968
TC5	1.594	29.35	2.4222	21.497
TC6	4.254	113.6	4.2647	49.404

```
CEL:
  &replace EXPRESSIONS:
    Freq = 170[GHz]
    P0 = 0.465[MW]
1   RhoECuCrZn = 6.76e-11[Ohm*m/K]*(T-273.15[K])+2.03e-8[Ohm*m]
    Z0 = 120*pi [Ohm]
    a = 0.025 [m]
2   fOmega = 4*s*sqrt(pi*RhoECuCrZn/(lambda*Z0))*((cos(phi/2))^-1)
    flowrate = 0.18[kg/s]
    lambda = clight/Freq
    phi = 90[degree]*pi[rad]/180[degree]
    rr = sqrt(x^2+y^2)
    s = 1
3   Q0 = if(rr<a&&rr>-a,q0,0[W*m^-2])

4   q0 = ((P0*fOmega*3.71*cos(phi/2))/(pi*a^2))*(besselJ(0,((r/a)*2.405)))^2
5   q1 = fOmega*cos(phi/2)

  END
 END
END
```

Fig. 23. List of expressions inserted in CFX to describe the heat applied on the mirror surface. In the centered heat flux, the Q0 (Eq. (3)) is used; while for the off centered beam case the intensity is inserted as a function of its location on the mirror surface, then is multiplied by the loss factor (Eq. (5)).

off-center beam. Again, their fast time response might allow them to be used for final alignment of the injected gyrotron beam, at relatively short pulse length, especially if more than one MB mirror is equipped with TCs and provided that the higher-order modes are dominantly resulting from the injected beam (e.g. the MBs should not be too distant from the input so that any potential higher-order mode content generated by the preceding transmission line misalignment, such as sagging or coupling errors (e.g. tilts/offsets), are negligible). Future configurations of the FALCON facility will implement a second instrumented MB mirror.

Conflict of interest

The authors declare no conflict of interest.

Declaration of Competing Interest

The authors report no declarations of interest.

Acknowledgements

This work has been carried out in the context of F4E framework contract OFC-671-TO4 which has been funded with support from Fusion from Energy. The views and opinions expressed herein do not necessarily reflect those of the European Commission, Fusion for Energy or the ITER organization.

Appendix A

A.1 Thermal loads on a mirror

A.1.1 Ohmic dissipation of microwaves at the reflecting surface

The ohmic loss depends on the surface resistance of the reflector as well as the polarization of the incident wave. For E-plane polarized waves (electric field vector lies on the plane formed by the normal to the reflecting surface and wave-vector of the incident radiation) the fractional lost power, $f_{\Omega E}$, is given by

$$f_{\Omega E} = 4 \cdot S_{\text{eff}} \sqrt{\frac{\pi \cdot \rho_e}{\lambda \cdot Z_0}} \frac{1}{\cos\frac{\theta}{2}} \tag{1}$$

Where:

- S_{eff} is a surface factor that takes into consideration the surface roughness, micro-cracks, impurities, etc. In the current case the s is taken equal to 1.44.
- ρ_e is the temperature dependent electrical resistivity of the facing component. In our case the Mirror Material is CuCrZr, with ρ_e equal to:

$$\rho_e = 6.76e^{-11} \cdot T + 2.03e^{-8}\ [\text{Ohm} \cdot \text{m/K}] \tag{2}$$

- Z_0 is the impedance of the free space ($\sqrt{\frac{\mu_0}{\epsilon_0}} = c \cdot \mu_0 \approx 120 \cdot \text{pi}$)

- θ is the total bend angle, which for MB equals 90 °.

Similarly, for H-plane incidence (the electric field lies perpendicular to the plane formed by the normal to the reflecting surface and the wave-vector of the incident radiation), the fractional lost power, $f_{\Omega H}$, is given by:

$$f_{\Omega H} = 4 \cdot S_{\text{eff}} \sqrt{\frac{\pi \cdot \rho_e}{\lambda \cdot Z_0}} \cdot \cos\frac{\theta}{2} \tag{3}$$

The difference between the two formulae is in the angular dependence. For electron cyclotron heating and current drive, the wave launched into the plasma must be circularly polarized to be completely absorbed. The launched wave will thus contain both E and H-plane components. The mirror is designed for the most demanding case where the polarization must be calculated for $f_{\Omega H} = 0$ and consequently $f_{\Omega} = f_{\Omega E}$.

A.1.2 Bessel profile

The magnitude of the electric field within the WG is given by

$$E_{(r)} = \frac{1}{a}\sqrt{\frac{2}{\pi} \cdot P_{\text{tot}} Z_0} \cdot \frac{J_0 \cdot \left(\frac{r}{a} \cdot 2.405\right)}{J_1 \cdot (2.405)} \tag{4}$$

Where:

- a is the WG radius, which in our case is equal to 0.025 m;
- P_{tot} is the total incident beam power (typically 1 MW at 170 GHz), in the current FEA model P_{tot} is taken equal to 0.465 MW in order to have a direct comparison with the experimental set up;
- J_0 is the Bessel function of order 0, calculated for the normalized radius $\rho = \chi \cdot r/a$. This function has a value 1 on axis $(r = 0)$ and zero at $r/a = 1$; $\chi = 2.405$, the first zero of the Bessel function.
- J_1 is the Bessel function of order 1, calculated at the first 0 of J_0, which is 2.405.

The power density $I_{(r)}$ for a HE_{11} mode in a corrugated WG is according to the Eq. (5):

$$I_{(r)} = P_{\text{tot}} \frac{3.71}{\pi a^2} \cdot J_0^2\left(\frac{r}{a} \cdot 2.405\right) \cdot \tag{5}$$

where the factor of $J_1^2(2.405)$ is the normalization (peaking factor) from the Bessel function dependence of the HE_{11} mode. The peak power density determines the critical heat flux for the cooling system. The peak absorbed power density which corresponds to the peak incident surface heat flux, q_s, is given at $r = 0$ for E-plane polarized waves, with (Eq. (1)),

$$q_s = P_{\text{tot}} \frac{3.71}{\pi} \cdot f_{\Omega E} \tag{6}$$

A.1.3 List of expressions in CFX which calculate the heat loss on the surface of the mirror

The equations mentioned in A.1 are given as input expressions in CFX as shown in Fig. 23. The *rr* parameter which is included in the Bessel function describes a circular domain; the heat flux is applied on a local coordinate system which is rotated by 45° and considers the projection of the circular domain, an ellipse.

References

[1] P.S. Silva, R. Chavan, M. Gagliardi, T. Goodman, J.-D. Landis, F. Ramseyer, A. M. Sanchez, M. Vagnoni, Thermal mechanical analyses of the mm-wave miter bend for the iter electron cyclotron upper launcher first confinement system https://www.ansys.com/, Fusion Eng. Des. 136 (2018) 650–654.

[2] https://www.ansys.com/.

[3] M. Henderson, R. Heidinger, D. Strauss, R. Bertizzolo, A. Bruschi, R. Chavan, E. Ciattaglia, S. Cirant, A. Collazos, I. Danilov, et al., Overview of the iter ec upper launcher, Nucl. Fusion 48 (5) (2008) 054013.

[4] C. Lau, M.C. Kaufman, E. Doyle, G.R. Hanson, W. Peebles, G. Wang, A. Zolfaghari, Circular corrugated miter bend and gap losses for broadband frequency applications, IEEE Trans. Microw. Theory Tech. 67 (1) (2018) 38–49.

[5] J. Doane, J. Anderson, H. Grunloh, W. Wu, Power monitor miter bends for high-power microwave transmission, Fusion Eng. Des. 93 (2015) 1–8.

[6] M.K. Thumm, W. Kasparek, Passive high-power microwave components, IEEE Trans. Plasma Sci. 30 (3) (2002) 755–786.

[7] A.M. Sánchez, R. Chavan, D. Dall'Acqua, M. Gagliardi, T. Goodman, J.P. Cansino, E.R. Ordoñez, G. Saibene, P. Wouters, Numerical analyses of the monoblock mitre bend for the iter electron cyclotron upper launcher, Fusion Eng. Des. (2021) same proceedings.

[8] H. Hailer, G. Dammertz, V. Erckmann, G. Gantenbein, F. Hollmann, W. Kasparek, W. Leonhardt, M. Schmid, P. Schüller, M. Thumm, M. Weissgerber, Mirror development for the 140 ghz ecrh system of the stellarator w7-x, Fusion Eng. Des. 66-68 (2003) 639–644, https://doi.org/10.1016/S0920-3796(03)00264-3, 22nd Symposium on Fusion Technology.

[9] W. Kasparek, L. Empacher, V. Erckmann, G. Gantenbein, F. Hollmann, H. Laqua, P. Schüller, M. Weißgerber, H. Zohm, Mirror development for the 140 ghz ecrh transmission system on the stellarator w7-x, Fusion Eng. Des. 53 (1) (2001) 545–551, https://doi.org/10.1016/S0920-3796(00)00532-9.

[10] T. Goodman, M. Cavinato, R. Chavan, A. Más-Sanchez, P.S. Silva, M. Vagnoni, T. Tersztyanszky, S. Carre, High-power testing of guided-wave components for the iter ech upper launcher at the falcon test facility, IEEE Trans. Plasma Sci. 48 (2020) 1537–1542.

[11] E.J. Kowalski, D.S. Tax, M.A. Shapiro, J.R. Sirigiri, R.J. Temkin, T.S. Bigelow, D. A. Rasmussen, Linearly polarized modes of a corrugated metallic waveguide, IEEE Trans. Microw. Theory Tech. 58 (11) (2010) 2772–2780.

[12] A. Chirkov, G. Denisov, N. Aleksandrov, 3d wavebeam field reconstruction from intensity measurements in a few cross sections, Opt. Commun. 115 (5-6) (1995) 449–452.

[13] Y. Oda, K. Kajiwara, K. Takahashi, A. Kasugai, M.A. Shapiro, R.J. Temkin, K. Sakamoto, Measurement of rf transmission mode in iter relevant ec h&cd transmission line, J. Infrared Millim. Terahertz Waves 31 (8) (2010) 949–957.

[14] W. Bin, A. Bruschi, F. Fanale, M. Francesca, F. Lucca, F. Albajar, S. Alberti, G. Carannante, M. Cavinato, I. Chelis, et al., Tests and developments of a long-pulse high-power 170 ghz absorbing matched load, Fusion Eng. Des. 146 (2019) 36–39.

[15] R. Atroshenkov, G. Kalinin, V. Barabash, Appendix a, materials design limit data. In-vessel Components, SDC-IC, ITER v3.3, 2013.

[16] F. Menter, Zonal two equation k-ω turbulence models for aerodynamic flows, 23rd Fluid Dynamics, Plasmadynamics, and Lasers Conference (1993) 2906.